Journal of Biomedical Optics

BiomedicalOptics.SPIEDigitalLibrary.org

Photoacoustic molecular imaging for *in vivo* liver iron quantitation

Federica Maccarinelli
Fernando Carmona
Maria Regoni
Paolo Arosio

Maccarinelli, F.; et al. Photoacoustic molecular imaging for in vivo liver iron quantitation. Journal of Biomedical Optics 21(5): 056008 (2016). (Mar 1, 2016).
DOI: http://dx.doi.org/10.1117/1.JBO.21.5.056008

SPIE.

Federica Maccarinelli, Fernando Carmona, Maria Regoni, Paolo Arosio, "Photoacoustic molecular imaging for *in vivo* liver iron quantitation," *J. Biomed. Opt.* **21**(5), 056008 (2016), doi: 10.1117/1.JBO.21.5.056008.

Photoacoustic molecular imaging for *in vivo* liver iron quantitation

Federica Maccarinelli, Fernando Carmona, Maria Regoni, and Paolo Arosio*
University of Brescia, Department of Molecular and Translational Medicine, Laboratory of Molecular Biology, Viale Europa 11, Brescia 25123, Italy

Abstract. A recent study showed that ferritin is a suitable endogenous contrast agent for photoacoustic molecular imaging in cultured mammalian cells. We have therefore tested whether this imaging technique can be used for *in vivo* quantification of iron in mouse livers. To verify this hypothesis, we used multispectral optoacoustic tomography (MSOT) to image albino CD1 mice before and after experimental iron loading. Postmortem assays showed that the iron treatment caused a 15-fold increase in liver iron and a 40-fold increase in liver ferritin levels, while *in vivo* longitudinal analysis using MSOT revealed just a 1.6-fold increase in the ferritin/iron photoacoustic signal in the same animals. We conclude that MSOT can monitor changes in ferritin/iron levels *in vivo*, but its sensitivity is much lower than that of *ex vivo* iron assays. [DOI: 10.1117/1.JBO.21.5.056008]

Keywords: photoacoustic; iron; ferritin; multispectral optoacoustic tomography.

Paper 160124RR received Mar. 1, 2016; accepted for publication May 11, 2016; published online May 27, 2016.

1 Introduction

Noninvasive *in vivo* evaluation of tissue iron concentration in animal models is important for the study of iron-related disorders and their treatments.[1] Presently, magnetic resonance imaging (MRI) is the gold standard technique for tissue iron quantification *in vivo*. It measures iron indirectly by its effect on the $T1$, $T2$, and $T2*$ relaxation times of water.[2] Since most of the nonheme iron deposited in the tissues is stored inside the ferritin, and ferritin can be detected by photoacoustic devices, it was recently proposed by the use of photoacoustic molecular imaging (PMI) techniques to detect endogenous ferritin *in vivo*.[3] Multispectral optoacoustic tomography (MSOT) is emerging as a powerful noninvasive PMI technique for resolving tissue chromophores at the high spatial resolution provided by ultrasound detection,[4,5] thus becoming an alternative technique for *in vivo* imaging in small animals.[4] The method is based on the measure of the acoustic waves generated by the thermoelastic expansion of the environment surrounding molecules that absorb an electromagnetic radiation. The amplitude of the generated acoustic waves depends on the optical absorption profile of the tissue.[6] When the emitted acoustic waves reach an ultrasound detector, they can be combined for the reconstruction of high-resolution images deep in tissue, since ultrasonic scattering is about two to three orders of magnitude weaker than optical scattering.[7,8] *In vivo*, the system needs probes that absorb in the near-infrared (NIR) region, as these wavelengths are able to penetrate through the tissues up to 1 cm deep. For example, oxy- and deoxy-hemoglobin are important endogenous chromophores with absorption bands in the NIR region that have been used to monitor blood flow and angiogenesis using photoacoustic approaches.[9] Other endogenous photoacoustic probes present *in vivo* include melanin, bilirubin, and lipids.[10] Melanin is located in the skin of nonalbino mice, bilirubin can be detected in the lumen of the intestine, and lipids show a photoacoustic signal at wavelengths above 900 nm. Recently, it was shown that ferritin overexpressed in cultured cells can be monitored by PMI due to its capacity to form an iron core that absorbs in the infrared region.[3] This observation prompted us to verify whether ferritin can also be used as an *in vivo* endogenous probe, based on the fact that ferritin evaluation gives a reliable index of iron loading because its expression is strongly stimulated by iron, particularly in the liver.[11] In the present work, we used MSOT to detect and quantify liver ferritin/iron accumulation *in vivo* in mice before and after experimental iron loading.

2 Materials and Methods

2.1 *Multispectral Optoacoustic Tomography*

All MSOT experiments were performed using an inVision-128 small animal scanner (iThera Medical GmbH, Munich, Germany). The excitation laser produces light pulses in the NIR range (680 to 980 nm) at a repetition rate of 10 Hz and the acoustic waves generated are detected by a 270-deg ultrasound transducer array with a central frequency of 5 MHz, suitable for imaging at depth required for an entire mouse cross section. The transducer has a center frequency of 5 MHz $\pm 10\%$ and a bandwidth of $>60\%$ in receive mode only. This allows practical acquisition of signals between 50 kHz and 7 MHz and provides an in-plane spatial resolution of 165 μm. There is an impulse response correction, and the data are further filtered to keep only the range 10 KHz to 10 MHz. During image acquisition, the artificial devices or mice were moved through the transducer array to capture the corresponding transverse image slices. Multispectral data analysis occurs in two regimes: online (during acquisition) and offline (postprocessing). The online analysis depends on the real-time backprojection reconstruction algorithm. Further, it uses the linear regression algorithm for spectral unmixing to resolve individual components from different chromophores in the system. For each

*Address all correspondence to: Paolo Arosio, E-mail: paolo.arosio@unibs.it

1083-3668/2016/$25.00 © 2016 SPIE

pixel in the image, the method fits the total measured optoacoustic spectrum to the known absorption spectra of the individual chromophores, based on least-squares linear regression.[12]

2.1.1 *Phantom*

Phantoms used in this study are artificial devices that simulate the shape, size, and optical properties of mouse body in imaging techniques. They were made of 1.5% agar, 1% lipid content[13,14] with 2 cm in diameter holding two inner channels (3-mm diameter) with the sample and the control placed separately in two transparent plastic straws (volume ~250 μL). No absorbent was added to the phantom mixture to better mimic *in vivo* tissues. Twofold serial dilutions of iron (iron-dextran solution 12.5 mg/mL, Sigma) and ferritin (ferritin from horse spleen 0.38 mg/mL, Sigma) were inserted in scattering agar phantoms using water as control. Phantoms were scanned at excitation wavelengths from 680 to 980 nm with a stepwise increment of 10 nm using three average frames per illumination wavelength then averaged to create a single image. MSOT acquisition was performed in three transverse planes (~800 μm cross section) with a step size of 2 mm across the phantom. For quantitative calculation, the iron/ferritin photoacoustic signal was obtained from the region of interest (ROI) area drawn in correspondence of the samples using the transverse photoacoustic images provided by ViewMSOT™ 3.6 software.

2.1.2 *Mice and iron treatment*

All the procedures followed animal protection laws and institutional guidelines of the European Convention for the Protection of Laboratory Animals. The study was approved by the Institutional Animal Care and Use Committee of the University of Brescia and the Italian Ministry of Science and Research. We used six female CD1 albino background mice that were 5 weeks old. A group of three mice was treated intraperitoneally with 5 mg of iron (iron-dextran solution, Sigma) twice a week for three consecutive weeks and three control mice were treated with saline in the same way. MSOT acquisition was performed for all the mice before the treatment and every week 2 days after the second weekly injection. The animals were anesthetized for all imaging procedures by general isoflurane anesthesia (1.8% to 2.0% at 0.8 L/min). The anesthetized mice were shaved and their skin surface was covered with an ultrasound gel, then they were placed in the instrument in horizontal position and wrapped in a thin polyethylene membrane. Imaging was performed on transverse slices with a step size of 0.5 mm from the end of the rib cage to the end of the kidneys using 20 average frames per illumination wavelength at 700, 730, 760, 800, and 850 nm to obtain a spectral unmixed image of a cross section every 10 s. Averaging pertains to the number of sequential laser pulses that are "averaged" into a single data point before the laser continues to the next defined wavelength. In principle, averaging increases the contrast-to-noise ratio for a given acquisition or to account for motion, but averaging is also a determinant of temporal resolution. For most *in vivo* applications, using 20 averages is a good compromise between increasing contrast to noise as well as accounting for motion related to breathing (typically 1 Hz) on the one side and good temporal resolution on the other side. For anatomical localization of the signal, the transverse photoacoustic images at 850 nm were compared with the mouse atlas provided by ViewMSOT™ 3.6 software. For quantitative calculation of the ferritin/iron photoacoustic signal, a similar ROI area was drawn over the liver.

2.2 *Biochemical Analysis*

2.2.1 *Tissue preparation*

Mice were anesthetized with Avertine (23-μL/g mouse; Sigma), sacrificed, and perfused with a physiological saline solution containing 2% heparin; tissue samples were then removed and lysed in ice-cold lysis buffer (20-mM Tris buffer, pH 7.4, 1% Triton X-100, 1-mM sodium azide, 1-mM PMSF, 10-mM leupeptin, and 1-mM pepstatin) using a Potter homogenizer. The homogenates were clarified by centrifugation at 10,000 g for 10 min at 4°C, and the supernatant proteins were quantified by Bradford assay (Biorad).

2.2.2 *Ferritin immunoblot*

Protein extracts (30 μg) were separated by 12% sodium dodecyl sulfate polyacrylamide gel electrophoresis and transferred onto nitrocellulose membranes (GE Healthcare). Immunoblotting was performed using specific primary antibodies antiferritin (Sigma) and anti-GAPDH (Sigma). After incubation with horseradish peroxidase-conjugated secondary antibodies, the bands were revealed by enhanced chemiluminescence (ECL from GE Healthcare) and quantified by densitometry analysis using ImageJ software.

2.2.3 *Iron assay*

Photometric iron evaluation was done as described in Ref. 15. Briefly, 50 mg of liver tissue were digested in an acidic solution (HCl 3 M and trichloroacetic acid 0.6 M) at 65°C for 16 h. Then, samples were clarified by centrifugation and 10 μL of the supernatant were added to 240 μL of working chromogen reagent (0.01% bathophenanthroline and 0.1% thioglycolic acid in 45% sodium acetate). The solutions were then incubated for 30 min at room temperature until color development and the absorbance measured at 535 nm.

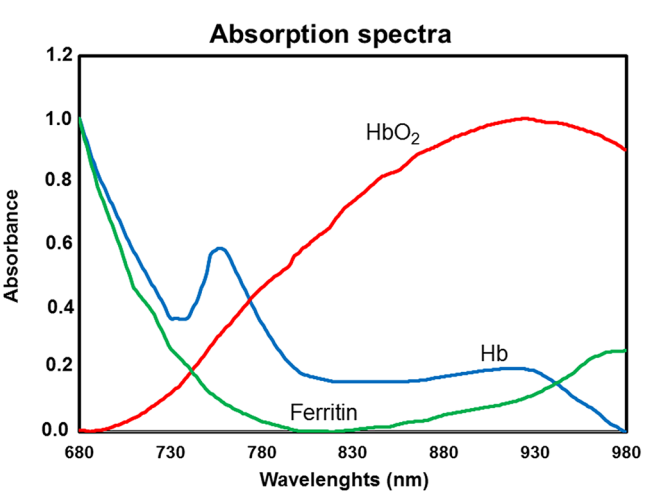

Fig. 1 NIR absorption spectra of ferritin, Hb, and HbO_2. The absorption and the photoacoustic spectra of ferritin and Hb in the 680 to 900 nm range are similar with the exception of an Hb peak at 760 nm, while the HbO_2 spectrum shows a wide absorption peak at higher wavelengths.

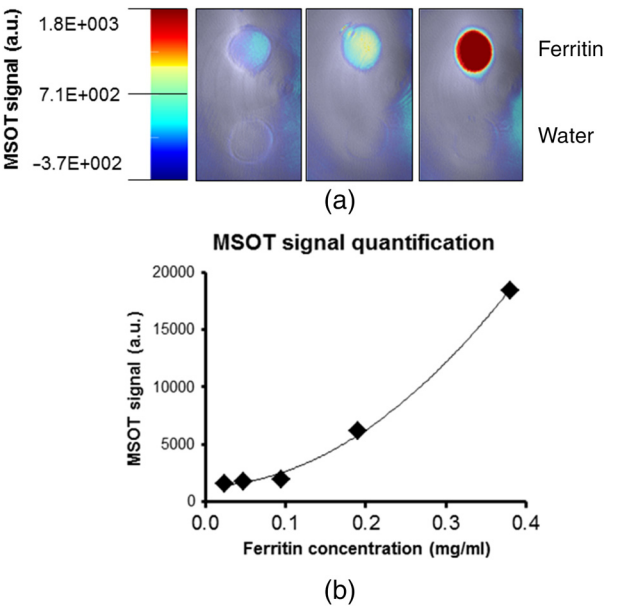

Fig. 2 Photoacoustic properties of ferritin/iron. (a) Photoacoustic tomographically reconstructed images. Ferritin dilutions were inserted in a scattering and nonabsorbing tissue-mimicking phantom device using water as control. (b) Photoacoustic signal quantification of ferritin. The ferritin/iron photoacoustic signal was obtained from the ROI area drawn in correspondence of the samples using the transverse photoacoustic images provided by ViewMSOT™ 3.6 software. The graph shows the relationship between the MSOT signal and the ferritin concentration (95 to 380 μg/mL).

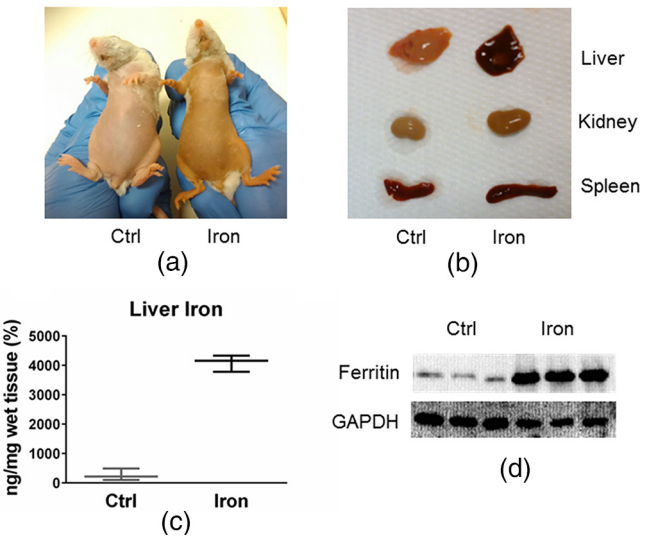

Fig. 4 Analysis of the iron-treated and untreated mice. (a) The skin color of the shaved mice after the 3-week iron treatment was darker than that of the controls. (b) After the sacrifice, tissue samples were collected for biochemical analysis. A darker color in the liver of iron-treated mice is evident compared to the controls, while the color of the kidney is similar, indicating the correct perfusion of the animals. (c) Photometric iron evaluation shows a 15-fold increase of the liver nonheme iron concentration in the treated mice. (d) Immunoblotting on liver protein extracts, performed using the specific primary antibody, shows a 40-fold ferritin increase in iron-loaded mice.

3 Results and Discussion

Ferritin photoacoustic properties were recently analyzed *in vitro* in cells[3] in the absence of hemoglobin (Hb) and oxygenated hemoglobin (HbO_2), the two main endogenous iron-containing *in vivo* photoacoustic absorbers.[16] Thus, we started comparing the photoacoustic properties of iron-loaded ferritin with those of the Hbs. The absorption spectra of ferritin and Hb in the 680 to 900 nm range are similar with the exception of an Hb peak at 760 nm, while the HbO_2 spectrum shows a wide absorption peak at higher wavelengths (Fig. 1).

For signal deconvolution, the ViewMSOT™ 3.6 software provided by the inVision-128 small animal scanner uses a linear algorithm. Unmixing the ferritin signal from that of HbO_2 does not pose problems, while the unmixing from that of Hb may suffer of some limitations, since it is based only on the difference at 760 nm between their absorption spectra. Then, to verify whether ferritin/iron can be monitored by MSOT using our equipment (inVision-128 small animal scanner), twofold serial dilutions of ferritin and iron dextran were loaded in a scattering and nonabsorbing tissue-mimicking phantom device using water as the control reference. In the concentration range compatible with that expected in some tissues of living mice (95 to 380 μg/mL),[17] the MSOT signal obtained was positively related to the loaded concentration of ferritin (Fig. 2) and iron (data not shown). The relationship between the photoacoustic signal

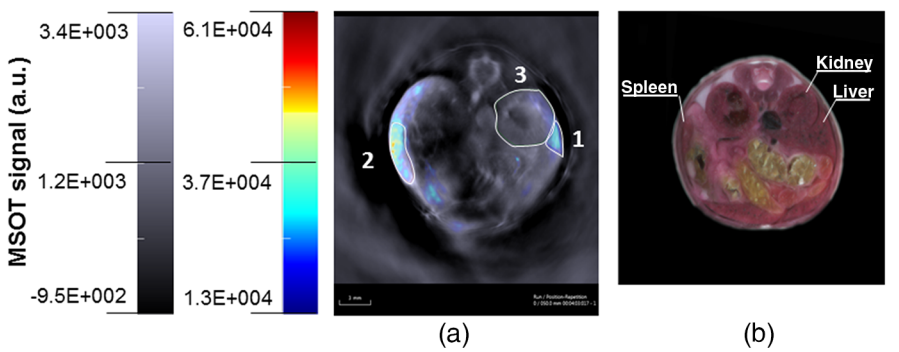

Fig. 3 *In vivo* photoacoustic tomographically reconstructed image of a transverse slice of an untreated mouse. (a) The grayscale image represents a single wavelength (850 nm) and was used as background for the anatomical localization of the signal. The colored scale shows the ferritin/iron photoacoustic signal. All the mice show a stronger ferritin signal (1) in the liver and (2) in the spleen. On the contrary, no ferritin absorbance was detected (3) in the kidneys. (b) Corresponding transverse image of the mouse atlas provided by ViewMSOT™ 3.6 software.

obtained with the MSOT and the ferritin/iron concentration supported the possibility to use ferritin as an endogenous photoacoustic contrast agent *in vivo* in mice.

Next, we analyzed six untreated mice of the CD1 albino background using the settings for ferritin/iron detection. The anatomical localization of the signal was obtained comparing the photoacoustic background image at 850 nm, where no ferritin/iron photoacoustic signal is present, with the corresponding transverse image of the mouse atlas provided by the ViewMSOT™ 3.6 software. This allowed precise drawing of ROI areas over the liver, spleen, and other organs, for the quantitation of the photoacoustic signal. An evident ferritin/iron photoacoustic signal was found in correspondence of the liver and spleen (Fig. 3), which are the major iron storage organs, but was not found in the kidneys and the heart (data not shown).

This result suggested that ferritin/iron could be quantified in the liver of living mice by photoacoustic analysis. To verify this, three CD1 mice were treated intraperitoneally (IP) with iron-dextran solution (5 mg/IP, twice a week for three consecutive weeks) to induce iron overload, while the other three control mice were treated in the same way with saline solution. The skin color of the shaved iron-loaded mice at the end of the treatment was darker than that of the saline-treated ones (Ctrl) [Fig. 4(a)], and after the sacrifice the liver of iron-treated mice showed a color remarkably stronger than that of the matched controls [Fig. 4(b)].

In addition, postmortem analyses showed that nonheme iron content in liver was 15-fold higher in iron-treated mice compared to the controls [Fig. 4(c)], and the ferritin level measured by western blotting was about 40-fold above the basal level [Fig. 4(d)]. Altogether, the biochemical analyses confirmed that the iron treatment was effective and induced a massive iron loading in the liver. MSOT acquisition was performed for all the mice before, during, and at the end of the treatment, before the sacrifice. Figure 5 shows the MSOT cross sections of the mice after the 3-week iron treatment.

A photoacoustic signal is evident in the ROI areas drawn over the liver and spleen region confirming that the ferritin/iron deposits are actually detected by the system in

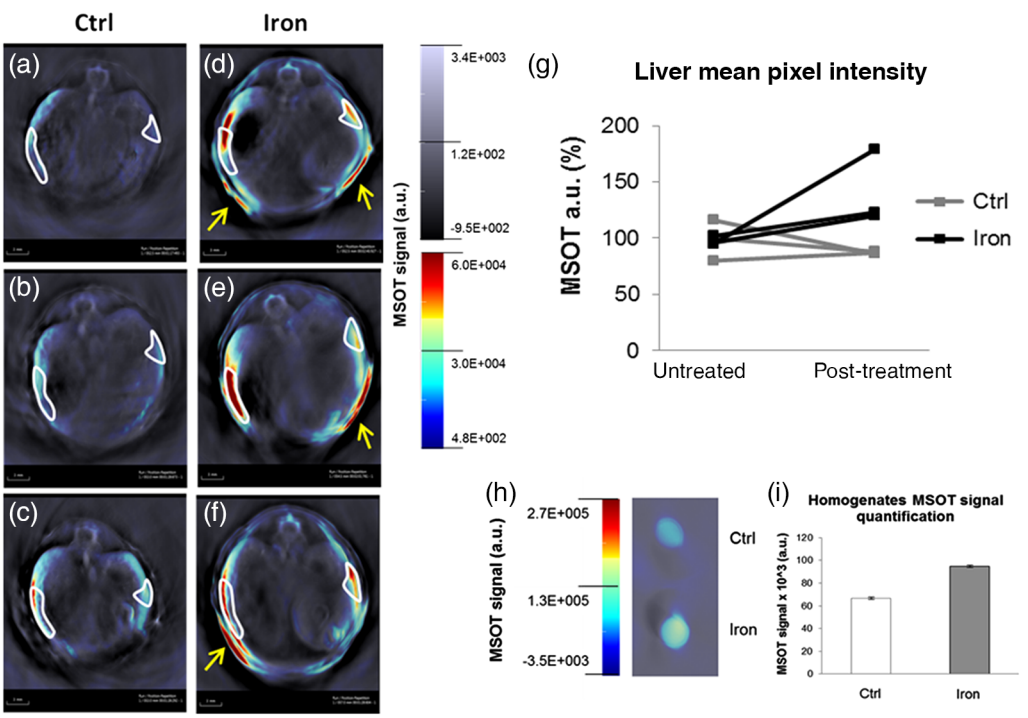

Fig. 5 *In vivo* and *ex vivo* photoacoustic analysis of the liver of iron-loaded and control mice. Photoacoustic tomographically reconstructed images of (d, e, f) iron-loaded mice show a stronger ferritin/iron signal both in the liver (right ROI) and in the spleen (left ROI) compared to (a, b, c) saline-treated mice. The gray-scale image taken at 850 nm was used for the anatomical localization of the signal. The colored scale shows the ferritin/iron photoacoustic signal. (g) Quantitation of the ferritin/iron photoacoustic signal was obtained from the ROI areas drawn over the liver using the transverse photoacoustic images provided by ViewMSOT™ 3.6 software. The mean photoacoustic signal of the liver of iron-treated animals was 1.6-fold higher than that of the control ones. A similar signal dispersion is observed in the iron-loaded mice before and after the treatment, while no differences are observed in the saline-treated ones. The iron-loaded mice showed an increase of the ferritin/iron photoacoustic signal also in peripheral areas in proximity of the liver and the spleen (yellow arrows). (h) Photoacoustic tomographically reconstructed images. Liver homogenates of iron-loaded and control mice were inserted in a scattering and nonabsorbing tissue-mimicking phantom. (i) Photoacoustic signal quantification of ferritin. The ferritin/iron photoacoustic signal was obtained from the ROI area drawn in correspondence of the samples using the transverse photoacoustic images provided by ViewMSOT™ 3.6 software. The graph shows a signal 1.5-fold higher in the iron-loaded mice compared to the controls, a difference not statistically significant.

physiological conditions [Figs. 5(a), 5(b), and 5(c)]. A careful quantification of the pixel intensity of the similar ROI areas showed that the signal of the three control mice did not change significantly during the period of the treatment, while that of the iron-treated animals increased. In two mice it increased about 20%, and in one mouse it increased about 90%, with a mean signal 1.6-fold higher in the iron-loaded mice compared to the controls, a statistically insignificant difference [Fig. 5(g)]. A similar increase in the photoacoustic signal was also found analyzing the liver homogenates inserted in an agar phantom [Fig. 5(h)]. The iron-loaded mice showed an increase of the ferritin/iron photoacoustic signal also in peripheral areas in proximity of the liver and the spleen [Figs. 5(d), 5(e), and 5(f) yellow arrows], which was attributed to the skin and probably not directly linked to the iron overload. We are not aware that iron overload may cause an accumulation of iron or NIR probes in the skin; thus, further experiments are needed to verify the reasons leading to an increase of the photoacoustic signal in the skin after iron treatment.

In conclusion, we found that although MSOT can detect *in vivo* ferritin/iron overload in mice liver and spleen, its sensitivity is far too low for many applications, and is not comparable to that of postmortem analyses. Therefore, it seems to us unlikely that photoacoustic tomography could replace MRI for *in vivo* analysis of iron status in mice using endogenous ferritin as a photoacoustic reporter. The low sensitivity of MSOT in this study may be due to the low ferritin/iron absorbance in the NIR region compared to the high background signal given by Hb, which interferes with that of the ferritin.

Acknowledgments

We are grateful to Dr. Thomas Sardella for the great help in the preparation of the work and to Dr. Edoardo Parella for the support in the use of multispectral optoacoustic tomography. The work was partially supported by PRIN10-11 grant to P.A. F.M. was partially supported by a fellowship by Consorzio Interuniversitario Biotecnologie. The authors declare that there are no conflicts of interest.

References

1. N. C. Andrews, "Iron homeostasis: insights from genetics and animal models," *Nat. Rev. Genet.* **1**(3), 208–217 (2000).
2. C. B. Sirlin and S. B. Reeder, "Magnetic resonance imaging quantification of liver iron," *Magn. Reson. Imaging Clin. North Am.* **18**, 359–381 (2010).
3. S. H. Ha, A. R. Carson, and K. Kim, "Ferritin as a novel reporter gene for photoacoustic molecular imaging," *Cytometry* **81**, 910–915 (2012).
4. R. A. Kruger et al., "Thermoacoustic molecular imaging of small animals," *Mol. Imaging* **2**, 113–123 (2003).
5. V. Ntziachristos and D. Razansky, "Molecular imaging by means of multispectral optoacoustic tomography (MSOT)," *Chem. Rev.* **110**, 2783–2794 (2010).
6. A. Taruttis et al., "Real-time imaging of cardiovascular dynamics and circulating gold nanorods with multispectral optoacoustic tomography," *Opt. Express* **18**, 19592–19602 (2010).
7. J. Yao and L. V. Wang, "Photoacoustic tomography: fundamentals, advances and prospects," *Contrast Media Mol. Imaging* **6**, 332–345 (2011).
8. L. V. Wang and S. Hu, "Photoacoustic tomography: in vivo imaging from organelles to organs," *Science* **335**, 1458–1462 (2012).
9. P. Hai et al., "Near-infrared optical-resolution photoacoustic microscopy," *Opt. Lett.* **39**, 5192–5195 (2014).
10. M. Schwarz et al., "Three-dimensional multispectral optoacoustic mesoscopy reveals melanin and blood oxygenation in human skin in vivo," *J. Biophotonics* **9**, 55–60 (2016).
11. P. M. Harrison and P. Arosio, "The ferritins: molecular properties, iron storage function and cellular regulation," *Biochim. Biophys. Acta* **1275**, 161–203 (1996).
12. C. J. Ho et al., "Multifunctional photosensitizer-based contrast agents for photoacoustic imaging," *Sci. Rep.* **4**, 5342 (2014).
13. H. J. van Staveren et al., "Light scattering in intralipid-10% in the wavelength range of 400–1100 nm," *Appl. Opt.* **30**, 4507–4514 (1991).
14. R. Michels, F. Foschum, and A. Kienle, "Optical properties of fat emulsions," *Opt. Express* **16**, 5907–5925 (2008).
15. A. Roetto et al., "Comparison of 3 Tfr2-deficient murine models suggests distinct functions for Tfr2-alpha and Tfr2-beta isoforms in different tissues," *Blood* **115**, 3382–3389 (2010).
16. S. Hu and L. V. Wang, "Photoacoustic imaging and characterization of the microvasculature," *J. Biomed. Opt.* **15**, 011101 (2010).
17. B. Clothier et al., "Genetic variation of basal iron status, ferritin and iron regulatory protein in mice: potential for modulation of oxidative stress," *Biochem. Pharmacol.* **59**, 115–122 (2000).

Biographies for the authors are not available.